Measurement of the branching fraction of the decay $J/\psi \to p\bar{p}\eta$

M. Ablikim *et al.*[*]
(BESIII Collaboration)

(Received 4 July 2024; accepted 29 September 2024; published 29 October 2024)

A high-precision measurement of the branching fraction of the decay $J/\psi \to p\bar{p}\eta$ is performed using $(10\,087 \pm 44) \times 10^6$ J/ψ events recorded by the BESIII detector at the BEPCII storage ring. The branching fractions of the two decays $J/\psi \to p\bar{p}\eta(\eta \to \gamma\gamma)$ and $J/\psi \to p\bar{p}\eta(\eta \to \pi^+\pi^-\pi^0)$ are measured individually to be $\mathcal{B}(J/\psi \to p\bar{p}\eta(\eta \to \gamma\gamma)) = (1.480 \pm 0.001 \pm 0.024) \times 10^{-3}$ and $\mathcal{B}(J/\psi \to p\bar{p}\eta(\eta \to \pi^+\pi^-\pi^0)) = (1.557 \pm 0.003 \pm 0.038) \times 10^{-3}$, where the first uncertainties are statistical and the second systematic. Both results are compatible within their uncorrelated systematic uncertainties. The combined result is $\mathcal{B}(J/\psi \to p\bar{p}\eta) = (1.495 \pm 0.001 \pm 0.023) \times 10^{-3}$, where the first uncertainty is the combined statistical uncertainty and the second one the combined systematic uncertainty of both analyses, incorporating correlations between them. In addition, the $p\bar{p}$ threshold region is investigated for a potential threshold enhancement, and no evidence for one is observed.

DOI: 10.1103/PhysRevD.110.072021

I. INTRODUCTION

The Standard Model of particle physics describes many aspects in the field of subatomic physics with high precision. However, in the nonperturbative regime of QCD, many details are still not understood, and not all experimental observations can be explained. In addition, accurate predictions for particle interactions, resonance spectra, and decay processes are difficult to obtain due to the non-Abelian character of the underlying theory. One example is the spectrum of the N^* states, the excited nucleon resonances. There are many N^* resonances predicted by various theoretical models, e.g., the constituent quark model [1] or Lattice QCD calculations [2]. However, only a few of them have been experimentally confirmed so far. Many N* resonances, listed in the review of the Particle Data Group (PDG) [3], have been reported only by one experiment and need confirmation. In many cases, the properties of the reported resonances are not precisely measured yet. The huge BESIII dataset allows high-precision studies of J/ψ decays, e.g., the determination of branching fractions $\mathcal{B}$ and also the study of the N^* spectrum.

In recent years, several experimental results have been published about an enhancement near the $p\bar{p}$ threshold in radiative charmonium decays $J/\psi \to \gamma p\bar{p}$ and $\psi' \to \gamma p\bar{p}$ [4,5]. However, comparable hadronic decays like $J/\psi \to X p\bar{p}$, where X represents either ω, π, or η, have not shown similar structures [6–9]. Other radiative decays into light hadrons like $J/\psi \to \gamma\eta'\pi^+\pi^-$ and $J/\psi \to \gamma K_S^0 K_S^0 \eta$ also show structures near the $p\bar{p}$ threshold [10–12]. Different theoretical interpretations of these structures have been proposed, such as a $p\bar{p}$ bound state with mass $m_X \approx 1.85$ GeV/c^2 [13,14] or as a glueball, which would explain the absence of these structures in hadronic decays [15,16]. An overview is given in the review [17]. Since data in the energy range close to the $p\bar{p}$ threshold are sparse, these models are not well constrained by data [18]. In addition to these explanations, other effects, such as final-state interaction, might occur in the $p\bar{p}$ system, which might contribute to enhancements near the $p\bar{p}$ threshold. Therefore, it is important to search for threshold enhancements with higher statistics in the decays $J/\psi \to p\bar{p}\eta$ and $J/\psi \to p\bar{p}\pi^0$ to better constrain the models.

In this work, the branching fractions of the decay of $J/\psi \to p\bar{p}\eta$ with $\eta \to \gamma\gamma$ or $\eta \to \pi^+\pi^-\pi^0$ are measured with greatly improved precision in comparison to the previous measurements. Currently, the world average listed by the PDG is dominated by the measurement taken at BESII, which measured $\mathcal{B}(J/\psi \to p\bar{p}\eta) = (1.91 \pm 0.02 \pm 0.17) \times 10^{-3}$ [19]. The present work improves upon the BESII measurement with the much larger dataset of BESIII; improved analysis techniques that result in reduced systematic uncertainties; and, crucially, an improved determination of the global reconstruction efficiency. The precision is improved by more than a factor of 10. The large number of events in this final state also allows the exploration of the threshold region.

[*]Full author list given at the end of the article.

Published by the American Physical Society under the terms of the Creative Commons Attribution 4.0 International license. Further distribution of this work must maintain attribution to the author(s) and the published article's title, journal citation, and DOI. Funded by SCOAP[3].

II. BESIII EXPERIMENT

The BESIII detector is a magnetic spectrometer [20] located at the Beijing Electron Positron Collider (BEPCII) [21]. The cylindrical core of the BESIII detector consists of a helium-based multilayer drift chamber (MDC), a plastic scintillator time-of-flight system (TOF), and a CsI(Tl) electromagnetic calorimeter (EMC), which are all enclosed in a superconducting solenoidal magnet providing a 1.0 T magnetic field (0.9 T in 2012). The solenoid is supported by an octagonal flux-return yoke with resistive plate chamber muon-identifier modules interleaved with steel. The acceptance for charged particles and photons is 93% over the 4π solid angle. The charged-particle momentum resolution at 1 GeV/c is 0.5%, and the specific energy loss ($\mathrm{d}E/\mathrm{d}x$) resolution is 6% for electrons from Bhabha scattering. The EMC measures photon energies with a resolution of 2.5% (5%) at 1 GeV in the barrel (end cap) region. The time resolution of the TOF barrel part is 68 ps, while that in the end cap region was 110 ps. The end cap TOF system was upgraded in 2015 with multigap resistive plate chamber technology, providing a time resolution of 60 ps, which benefits 87% of the data used in this analysis [22,23].

III. DATASETS

In this analysis, the complete J/ψ dataset of $(10\,087 \pm 44) \times 10^6$ J/ψ events recorded by the BESIII experiment in the years 2009, 2012, 2018, and 2019 is analyzed. The total number of J/ψ events is determined using inclusive hadronic J/ψ decays [24]. Additionally, the continuum dataset at center of mass (CM) energy $\sqrt{s} = 3.080$ GeV with an overall luminosity of 168.6 pb^{-1} is analyzed to estimate background contributions from QED processes, beam-gas interactions, and cosmic rays. To understand the reconstruction efficiency of the signal channel as well as the relevant resolutions and limitations of the detector, Monte Carlo (MC) simulations are used. The initial e^+e^- collision, including initial-state radiation, and the generation of the J/ψ meson are simulated using KKMC [25]. The J/ψ decay and subsequent decays are simulated with the event generator EVTGEN [26,27]. Interactions with the detector material are simulated using GEANT4 [28].

Several MC samples are used in this analysis. Two exclusive samples of 1×10^6 events were produced to determine the reconstruction efficiencies of the signal decays $J/\psi \to p\bar{p}\eta$, with the subsequent decays of either $\eta \to \gamma\gamma$ or $\eta \to \pi^+\pi^-\pi^0$ with $\pi^0 \to \gamma\gamma$. Since the distributions of the reconstructed data events deviate from pure phase space (PHSP), these MC samples are generated using a model obtained with an amplitude analysis, which will be described in Sec. VI. The decay distribution of the η into three pions follows the ETA_DALITZ model [26] of EVTGEN, which is adjusted to fit experimental data.

Additionally, an inclusive MC sample of 10×10^9 J/ψ events is used to identify possible background contributions. This sample is generated to match the number of BESIII J/ψ events and uses a combination of world average $\mathcal{B}$s from the PDG [3] and effective models from LUNDCHARM [29,30].

IV. EVENT SELECTION

The decay $J/\psi \to p\bar{p}\eta$ is reconstructed using the dominant η decays $\eta \to \gamma\gamma$ and $\eta \to \pi^+\pi^-\pi^0$, with the π^0 subsequently decaying into $\gamma\gamma$. Consequently, each event is required to contain at least two photons and two charged tracks in the decay $J/\psi \to p\bar{p}\eta$ with $\eta \to \gamma\gamma$ or four charged tracks in the decay $J/\psi \to p\bar{p}\eta$ with $\eta \to \pi^+\pi^-\pi^0$.

Charged tracks are required to be reconstructed within the acceptance of the MDC, satisfying $|\cos\theta| < 0.93$, with θ being the angle between the reconstructed track and the z axis, which is the symmetry axis of the MDC. Additionally, the distance of closest approach to the interaction point is required to be $|V_{xy}| < 1$ cm in the radial direction and $|V_z| < 10$ cm along the z axis. In the $\eta \to \pi^+\pi^-\pi^0$ channel, the particle identification (PID) system is used to distinguish protons and charged pions. This system combines measurements of the energy deposited in the MDC ($\mathrm{d}E/\mathrm{d}x$) and the flight time in the TOF to form likelihoods $\mathcal{L}(h)(h = p, K, \pi)$ for each hadron h hypothesis. Protons are identified by imposing the criterion $\mathcal{L}(p) > \mathcal{L}(\pi)$, while charged pions are identified by requiring $\mathcal{L}(\pi) > \mathcal{L}(p)$. Since no sizable kaon background channels could be identified, no requirement on the kaon likelihood is used. In the $\eta \to \gamma\gamma$ channel, no PID requirement is applied to the charged tracks, since using the kinematic fit already suppresses most of the background events.

The photons from η and π^0 decays are required to have an energy deposition of more than 25 MeV in the barrel part of the EMC ($|\cos\theta| < 0.8$) and more than 50 MeV in the end caps of the EMC ($0.86 < |\cos\theta| < 0.92$). The angle $\Delta\alpha$ between the photon and nearest charged track should be larger than 20° to exclude bremsstrahlung photons or hadronic split-offs from charged tracks, and especially antiproton interactions within the calorimeter. Furthermore, it is required that the EMC shower is within 700 ns after the time of the collision. Combinations in which both photons are detected in the end caps are also rejected, since this improves the overall mass resolution of the η and π^0 candidates.

The selected photons are combined into η and π^0 candidates, requiring the invariant mass $M_{\gamma\gamma}$ of the two photons to lie within wide mass windows of 200 MeV $\leq M_{\gamma\gamma} \leq 900$ MeV/c^2 for η and 80 MeV/$c^2 \leq M_{\gamma\gamma} \leq$ 180 MeV/c^2 for π^0. In the $\eta \to \pi^+\pi^-\pi^0$ decay channel, the invariant mass of the three pions $M_{\pi^+\pi^-\pi^0}$ must be within the range of $200\,\mathrm{MeV}/c^2 \leq M_{\pi^+\pi^-\pi^0} \leq 900\,\mathrm{MeV}/c^2$.

After the photon and track selection, a vertex fit is performed to ensure a common point of origin of all charged tracks. Next, a kinematic fit is performed constraining the initial 4-momentum of the J/ψ as well as the mass of the π^0 in the $\eta \to \pi^+\pi^-\pi^0$ channel. The mass of the η is unconstrained, because the $M_{\gamma\gamma/\pi^+\pi^-\pi^0}$ spectrum is used to determine the number of signal events. If there are multiple candidates per event, only the candidate with the minimum χ^2 value of the kinematic fit is selected. A very loose requirement on the χ^2 value is used to suppress background events.

V. BACKGROUND STUDIES

To identify possible background contributions from other J/ψ decays, the inclusive MC sample is used. The same selection criteria as for the signal channel are applied to identify the most relevant background channels surviving the event selection.

In the $\eta \to \gamma\gamma$ decay channel, a wide variety of background contributions is found, with most channels only contributing a few events each. The most prominent background channels involve either an intermediate charged or neutral Δ resonance, or a decay of $J/\psi \to p\bar{p}X$ with X being a light meson that decays further into a number of photons. About 21% of background events contain misidentified charged particles. All background categories are distributed smoothly throughout the $M_{\gamma\gamma}$ spectrum with no peaking behavior in the signal region. The amount of background events remaining in the signal region is about 4.3%.

In the $\eta \to \pi^+\pi^-\pi^0$ decay channel, three major background sources are identified. The most abundant channel is $J/\psi \to \Delta X$ with X being a light baryon. The second dominant background contribution is the direct production of the final state, $J/\psi \to p\bar{p}\pi^+\pi^-\pi^0$. Both channels are distributed smoothly throughout the $M_{\pi^+\pi^-\pi^0}$ spectrum. On the other hand, the decay $J/\psi \to p\bar{p}\omega(\omega \to \pi^+\pi^-\pi^0)$ has a sharp peak at the ω mass, which is well separated from the signal region. The events of the remaining channels (3.7% of all background events) are distributed smoothly as well. The amount of background events remaining in the signal region is with about 33%, significantly higher than for the $\eta \to \gamma\gamma$ final state.

Background contributions from the same signal channel but with other η decays are also studied. In the $\eta \to \gamma\gamma$ decay channel, two events from other η decays are found, which is negligible. In the $\eta \to \pi^+\pi^-\pi^0$ decay channel, a significant peaking background contribution of the process $J/\psi \to p\bar{p}\eta(\eta \to \pi^+\pi^-\gamma)$ is found. The inclusive MC sample is used to estimate the rate and distribution of these events within the signal region. Based on the ratio of the $\mathcal{B}$s, about 1.51% of the reconstructed events are from this process.

An additional source of background events is the process $e^+e^- \to \gamma^* \to p\bar{p}\eta$ without a J/ψ as an intermediate state. To determine the number of events from this source, the continuum data sample taken at the CM energy $\sqrt{s} = 3.080$ GeV is analyzed. The same selection criteria as for the signal process are applied, with the exception that the 4-momentum of the initial state in the kinematic fit is adjusted. The number of background events in the signal region is estimated to be $N_{\mathrm{QED}}^{3080} = 310 \pm 18$ in the $\eta \to \gamma\gamma$ channel and $N_{\mathrm{QED}}^{3080} = 49 \pm 8$ in the $\eta \to \pi^+\pi^-\pi^0$ channel. Scaling those numbers to the luminosity of the J/ψ dataset yields a background contribution of $N_{\mathrm{QED}}^{\eta\to\gamma\gamma} = 5454(317)$ events in the $\eta \to \gamma\gamma$ channel and $N_{\mathrm{QED}}^{\eta\to\pi^+\pi^-\pi^0} = 826 \pm 141$ events in the $\eta \to \pi^+\pi^-\pi^0$ channel. Since it is expected that the differences in efficiency and cross section between the two CM energies are much smaller than the statistical uncertainty, these factors are neglected.

VI. EFFICIENCY DETERMINATION

The reconstruction efficiency describes the probability that a signal event is reconstructed in the detector and survives the whole selection chain. It depends heavily on each event's position in the available PHSP, being drastically lower in regions that contain one or more charged particles with low momentum, dropping to nearly zero in regions with $p_p \leq 200$ MeV/c. Moreover, if the distribution of events deviates from the simple PHSP distribution, a simulation that accurately reproduces data is required to determine the correct efficiency. For this analysis, the framework COMPWA [31] is used. The physics model is described by using the helicity formalism where N^* resonances as intermediate states are included. The fit of the model to data is performed using events from the $\eta \to \gamma\gamma$ channel only, with the additional constraint on the η mass, since this provides an almost background-free sample. The amplitude structure is not expected to differ between the two analyzed η decay channels, so the model is used to generate a signal MC sample for both channels.

Figure 1 shows the distributions of the invariant mass of all three subsystems, $M_{p\eta}$, $M_{\bar{p}\eta}$, and $M_{p\bar{p}}$, together with the amplitude model and the PHSP distributed MC sample of the three-body final state. For all distributions, the amplitude model, which includes seven N^* resonances as intermediate states in the $\bar{p}\eta$ and $p\eta$ subsystems, provides a good description of the data. In particular, the double peak structure close to threshold dominating the whole distribution could be described well by a destructive interference of two N^* resonances, the $N(1535)$ and the $N(1650)$. The large deviation in the $p\bar{p}$ subsystem is described by the reflection caused by the N^* resonances. The amplitude model describes the density of the events in the available phase space well, and thus the efficiency is determined correctly.

The reconstruction efficiency is calculated with $\epsilon_{\mathrm{rec}} = N_{\mathrm{rec}}/N_{\mathrm{gen}}$, where N_{rec} represents the number of

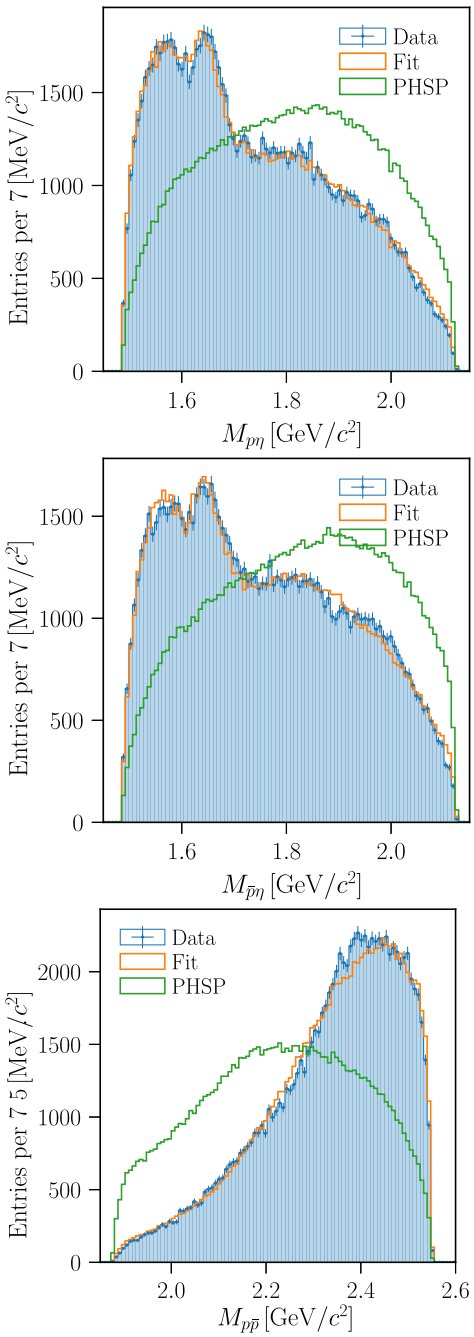


FIG. 1. The $M_{p\eta}$, $M_{\bar{p}\eta}$, and $M_{p\bar{p}}$ distributions in the $\eta \to \gamma\gamma$ decay channel from data (blue dots). The orange histogram shows the amplitude model, and the green histogram shows the distribution of the PHSP distributed MC sample.

reconstructed events and $N_{\rm gen}$ denotes the number of generated events. The reconstruction efficiency in the $\eta \to \gamma\gamma$ decay channel is determined to be $\epsilon_{\rm rec} = (44.17 \pm 0.04)\%$. In the $\eta \to \pi^+\pi^-\pi^0$ decay channel, the efficiency is $\epsilon_{\rm rec} = (16.40 \pm 0.04)\%$, which is considerably lower due to the additional charged particles from the η decay, which have comparatively low momentum.

VII. BRANCHING FRACTION

The branching fraction $\mathcal{B}$ of the signal decay is calculated by

$$\mathcal{B}(J/\psi \to p\bar{p}\eta) = \frac{N_{\rm Sig}}{N_{J/\psi}} \cdot \frac{1}{\epsilon_{\rm rec}} \cdot \frac{1}{\prod_i \mathcal{B}_i},$$

where $N_{\rm Sig}$ is the number of signal events, $N_{J/\psi}$ is the number of J/ψ events, $\epsilon_{\rm rec}$ is the reconstruction efficiency, and $\prod_i \mathcal{B}_i$ is the product of the branching fractions of the intermediate states, either $\mathcal{B}(\eta \to \gamma\gamma)$ or $\mathcal{B}(\eta \to \pi^+\pi^-\pi^0) \cdot \mathcal{B}(\pi^0 \to \gamma\gamma)$.

The number of signal events $N_{\rm Sig}$ is determined by counting the number of η candidates in the signal region of the $M_{\gamma\gamma}$ or $M_{\pi^+\pi^-\pi^0}$ distributions, after subtracting the estimated number of background events (see Fig. 2).

In the $\eta \to \gamma\gamma$ decay channel, the signal region is defined as 492 MeV/$c^2 \le M_{\gamma\gamma} \le$ 587 MeV/c^2 [inside the green

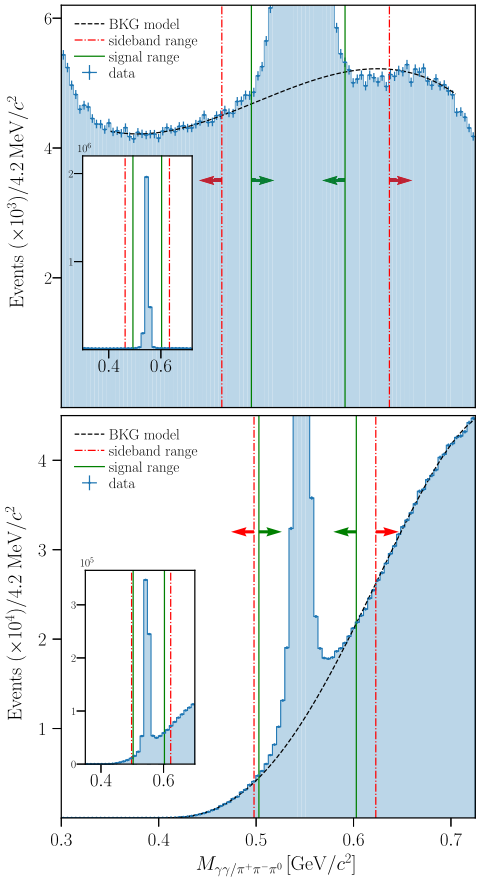


FIG. 2. Reconstructed $M_{\gamma\gamma}$ distribution of the $\eta \to \gamma\gamma$ decay channel (top) and reconstructed $M_{\pi^+\pi^-\pi^0}$ distribution of the $\eta \to \pi^+\pi^-\pi^0$ decay channel (bottom). The dashed black line describes the background (BKG) model. The dot-dashed red lines mark the boundaries of the sideband region, and the solid green lines mark the boundaries of the signal region. The insets show the complete distributions of the same data.

lines in Fig. 2(a)]. The sideband regions are defined as 350 MeV/$c^2 \leq M_{\gamma\gamma} \leq$ 462 MeV/c^2 and 632 MeV/$c^2 \leq M_{\gamma\gamma} \leq$ 700 MeV/c^2 [outside the red dot-dashed lines in Fig. 2(a)]. To estimate the number of background events, the sideband regions of the $M_{\gamma\gamma}$ distribution are fitted with a third-order Chebyshev function to describe the background shape, which is then interpolated to the signal region to calculate the background yield in that region. The fit yields $(11.20 \pm 0.04) \times 10^4$ background events in the signal region. Subtracting those as well as the expected 5454 ± 317 QED background events from the total number of $(271.60 \pm 0.16) \times 10^4$ events in the signal region gives the yield of $(259.85 \pm 0.117) \times 10^4$ signal events.

The fit procedure used in the $\eta \to \pi^+\pi^-\pi^0$ decay channel is similar. The total number of events in the signal region [502 MeV/$c^2 \leq M_{\pi^+\pi^-\pi^0} \leq$ 602 MeV/c^2, inside the green lines in Fig. 2(b)] is $(87.68 \pm 0.09) \times 10^4$. A fourth-order Chebyshev function is fitted to the background distribution of the sideband regions [407 MeV/$c^2 \leq M_{\pi^+\pi^-\pi^0} \leq$ 492 MeV/c^2 and 622 MeV/$c^2 \leq M_{\pi^+\pi^-\pi^0} \leq$ 725 MeV/c^2, outside the red dot-dashed lines in Fig. 2(b)], which yields $(28.37 \pm 0.04) \times 10^4$ background events in the signal region. After subtracting the yield of the background polynomial, the 826 ± 141 QED background events, and the estimated number of $(0.90 \pm 0.02) \times 10^4 \eta \to \pi^+\pi^-\gamma$ events, the signal yield is $(58.33 \pm 0.10) \times 10^4$ events.

With the numbers of signal events, the branching fractions are

$$\mathcal{B}(J/\psi \to p\bar{p}\eta(\eta \to \gamma\gamma)) = (1.480 \pm 0.001) \times 10^{-3},$$

$$\mathcal{B}(J/\psi \to p\bar{p}\eta(\eta \to \pi^+\pi^-\pi^0)) = (1.557 \pm 0.003) \times 10^{-3}.$$

The uncertainty reflects the statistical uncertainty from the number of signal events only. Table I shows the complete list of all relevant parameters.

TABLE I. The parameters used for the calculation of the branching fraction $\mathcal{B}$ measurements.

Parameter	Value
$N_{J/\psi}$ [24]	$(10\,087 \pm 44) \times 10^6$
$\mathcal{B}(\eta \to \gamma\gamma)$ [3]	$(39.36 \pm 0.18)\%$
$\mathcal{B}(\eta \to \pi^+\pi^-\pi^0)$ [3]	$(23.02 \pm 0.25)\%$
$\mathcal{B}(\pi^0 \to \gamma\gamma)$ [3]	$(98.823 \pm 0.0334)\%$
$N_{\mathrm{Sig}}(\eta \to \gamma\gamma)$	$(259.85 \pm 0.17) \times 10^4$
ϵ_{rec}	$(44.17 \pm 0.04)\%$
$N_{\mathrm{Sig}}(\eta \to \pi^+\pi^-\pi^0)$	$(58.33 \pm 0.10) \times 10^4$
ϵ_{rec}	$(16.40 \pm 0.04)\%$

VIII. STUDY OF THRESHOLD ENHANCEMENT

As shown in Fig. 1, the dynamics in the decay channel is dominated by processes like $J/\psi \to \bar{p}N^* \times (N^* \to p\eta) + c.c.$, with strong contributions of N^* resonances with relatively low mass. These contributions would be considered as background contributions for the study of a possible threshold enhancement in the $p\bar{p}$ system. Therefore, the kinematic regions of $M^2(p\eta) \geq 3.6$ GeV$^2/c^4$ and $M^2(\bar{p}\eta) \geq 3.6$ GeV$^2/c^4$ are chosen for this study because they do not show any obvious resonance contributions. Additionally, only events that satisfy $|M_{\gamma\gamma} - m_\eta| \leq 20$ MeV/c^2 are considered to reduce background contributions to a level of 1.8%. The impact of these requirements on the one-dimensional distribution of the invariant mass $M_{\bar{p}p}$ is substantial. Therefore, the ratio between the efficiency-corrected data distribution and the generated distribution of the PHSP MC dataset is shown in Fig. 3 as a function of the mass difference ΔM from the threshold. The ratio should be equal to 1 if no contribution from threshold enhancement or N^* resonances is present. In the low $\Delta M = M_{p\bar{p}} - 2m_p$ region, a ratio of greater than 1 would be expected in the presence of a threshold enhancement. In fact, the opposite behavior is observed, with the ratio between data and MC simulation being smaller than 1 in the vicinity of the threshold. This suggests either the absence of a threshold enhancement in the $p\bar{p}$ system, consistent with the previous results [6], or a complex interplay of the N^* and $p\bar{p}$ amplitudes.

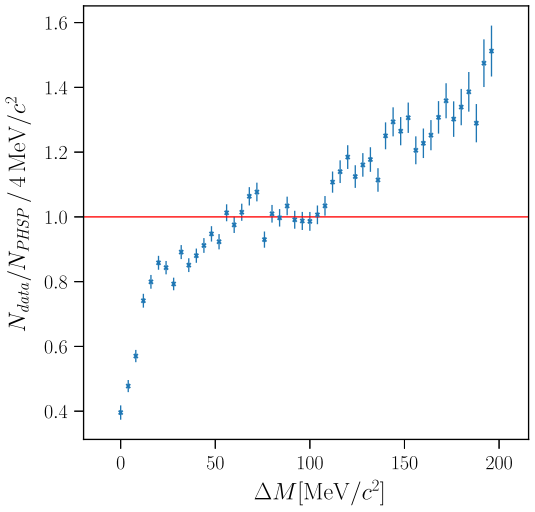


FIG. 3. Ratio between efficiency corrected $J/\psi \to p\bar{p}\eta$ data events N_{data} and with PHSP model generated MC events N_{PHSP} vs the mass difference to the production threshold $\Delta M = M_{p\bar{p}} - 2m_p$. Ratio of 1.0 is indicated by the red line.

IX. SYSTEMATIC UNCERTAINTY ESTIMATION

In the following, the different sources of the systematic uncertainties are described.

The systematic uncertainty of the track reconstruction efficiency is determined using a weighting method, which takes into account the dependence on the transverse momentum and the $\cos\theta$ of the tracks, when estimating the difference between data and MC simulation. The weights are obtained by studying the decay $J/\psi \to \pi^+\pi^- p\bar{p}$, which closely resembles the signal decay. The weighting is performed individually for every charged particle type, resulting in a total systematic uncertainty of 0.49% in the $\eta \to \gamma\gamma$ decay channel. In the $\eta \to \pi^+\pi^-\pi^0$ decay channel, the uncertainty for the protons is 0.47%, and the uncertainty for the pions is 0.78%.

The difference in the reconstruction efficiency of photons between data and MC simulation is studied with the decay channel $J/\psi \to \gamma\mu^+\mu^-$. The resulting systematic uncertainty is 0.5% per photon, or a total uncertainty of 1%.

The systematic uncertainty of the efficiency related to the particle identification in the channel with the $\eta \to \pi^+\pi^-\pi^0$ decay is determined also by using the weighting method and the channel $J/\psi \to \pi^+\pi^- p\bar{p}$. In this case, the dependence on the momentum and the $\cos\theta$ of the tracks is taken into account in estimating the difference between data and MC simulation. The weighting is performed individually for every charged particle type, resulting in a total systematic uncertainty of 1.02%. In the $\eta \to \gamma\gamma$ decay channel, no particle identification is used, and therefore no uncertainty is assigned.

The systematic uncertainty introduced by the veto on photon candidates, that are detected within a 20° cone around a charged track ($\Delta\alpha$), is estimated by varying the requirement by ±3°, which corresponds to taking into account the measurement of one less or one additional calorimeter crystal at low $\cos\theta$. The uncertainty is estimated to be 0.08% and 0.07% for the two channels, respectively.

The systematic uncertainty introduced by the requirement on the χ^2 value of the kinematic fit is estimated varying the requirement by ±10% and assigning the largest difference in $\mathcal{B}$ as the systematic uncertainty. It is estimated to be 0.11% and 0.17% for the two channels, respectively.

The statistical uncertainty of the reconstruction efficiency is treated as the systematic uncertainty for the branching fraction, with 0.09% in the $\eta \to \gamma\gamma$ channel and 0.25% in the $\eta \to \pi^+\pi^-\pi^0$ channel.

To estimate the systematic effects introduced by the choice of the boundaries of the signal and sideband ranges, each boundary is individually varied within ±10%. The exception to this is the lower boundary of the sideband range in the channel with the $\eta \to \pi^+\pi^-\pi^0$ decay, since it is already placed at the edge of the available phase space, so it is only varied upward. The largest difference in $\mathcal{B}$ for each category is assigned as the systematic uncertainty. All uncertainties are checked to see if they are already covered by statistical fluctuations by using the Barlow test [32]. Using this method, the following uncertainties are assigned of 0.01% (0.02%) for the lower bound of the signal range: 0.01% (0.04%) for the upper bound of the signal range, 0.03% (0.17%) for the width of the background window, 0.08% (0.54%) for the lower bound of the whole fit range, and 0.11% (0.37%) for the upper bound of the whole fit range, in the $\eta \to \gamma\gamma$ ($\eta \to \pi^+\pi^-\pi^0$) channel.

The shape of the background model is varied by changing the order of the polynomial function describing the background shape by plus/minus one order. The largest difference to the nominal value is taken as the uncertainty, which is 0.92% and 0.38% for the $\eta \to \gamma\gamma$ and the $\eta \to \pi^+\pi^-\pi^0$ channels, respectively.

The systematic uncertainty for the continuum background is calculated by Gaussian error propagation using the uncertainty of $N^{\rm QED}_{3080}$, which contributes an uncertainty of 0.01% in both channels.

The systematic uncertainty introduced by the determination of the amplitude model is estimated by varying the parameters of the model within the range taken from the covariance matrix. For 1000 different sets of parameters, the efficiency is determined, which results in a distribution of efficiency values. The standard deviation of this distribution is taken as the systematic uncertainty, which is 0.05% for the $\eta \to \gamma\gamma$ channel and 0.06% for the $\eta \to \pi^+\pi^-\pi^0$ channel.

For the external parameters such as the total number of J/ψ events and the branching fractions of the intermediate

TABLE II. Systematic uncertainties by source and the total systematic uncertainties. Uncertainties marked with (*) are considered correlated between the two channels.

Source	$\eta \to \gamma\gamma$	$\eta \to \pi^+\pi^-\pi^0$
$p\bar{p}$ tracks (*)	0.49	0.47
$\pi^+\pi^-$ tracks	…	0.78
Photons (*)	1.00	1.00
PID	…	1.02
$\Delta\alpha$ (*)	0.08	0.07
Kinematic fit	0.11	0.17
Efficiency	0.09	0.25
Signal range min	0.01	0.02
Signal range max	0.01	0.04
Background window	0.03	0.17
Fit range min	0.08	0.54
Fit range max	0.11	0.37
Background model	0.92	0.38
QED background	0.01	0.01
Amplitude model	0.05	0.06
$N_{J/\psi}$ (*)	0.43	0.43
$\mathcal{B}_\eta$	0.51	1.22
$\mathcal{B}_{\pi^0}$	…	0.03
Total	1.61	2.45

particles, Gaussian error propagation is used. For $N_{J/\psi}$, this results in a systematic uncertainty of 0.43% [24]; for $\mathcal{B}(\eta \to \gamma\gamma)$, it results in 0.51%; for $\mathcal{B}(\eta \to \pi^+\pi^-\pi^0)$, it results in 1.22%; and for $\mathcal{B}(\pi^0 \to \gamma\gamma)$, it results in 0.03% [3].

The total systematic uncertainties, which are listed in Table II, are calculated by summing all individual uncertainties in quadrature. The resulting relative systematic uncertainty is 1.61% for the $\eta \to \gamma\gamma$ decay channel and 2.45% for the $\eta \to \pi^+\pi^-\pi^0$ decay channel, which results in the absolute systematic uncertainties of 0.024×10^{-3} and 0.038×10^{-3}, respectively. Separating the correlated and uncorrelated systematic uncertainties, 0.018×10^{-3} corresponds in both cases to the correlated uncertainties.

The two measurements are combined taking into account the correlated and uncorrelated contributions to the systematic uncertainties of both channels [33]. The combined $\mathcal{B}$ is

$$\mathcal{B}(J/\psi \to p\bar{p}\eta) = (1.495 \pm 0.001 \pm 0.023) \times 10^{-3}.$$

The first uncertainty is the combined statistical uncertainty, and the second is the combined systematic uncertainty of both analyses.

X. CONCLUSIONS

This paper describes the most precise measurement to date of the branching fraction of the decay $J/\psi \to p\bar{p}\eta$, using the BESIII dataset of $(10\,087 \pm 44) \times 10^6$ J/ψ events. Two different η final states, $\eta \to \gamma\gamma$ and $\eta \to \pi^+\pi^-\pi^0$, are used for this analysis. The single branching fractions are determined to be

$$\begin{aligned}&\mathcal{B}(J/\psi \to p\bar{p}\eta(\eta \to \gamma\gamma))\\ &= (1.480 \pm 0.001 \pm 0.018 \pm 0.016) \times 10^{-3},\end{aligned}$$

$$\begin{aligned}&\mathcal{B}(J/\psi \to p\bar{p}\eta(\eta \to \pi^+\pi^-\pi^0))\\ &= (1.557 \pm 0.003 \pm 0.018 \pm 0.034) \times 10^{-3},\end{aligned}$$

where the first uncertainty is statistical and the second and third correspond to the correlated and uncorrelated systematic uncertainties, respectively. The difference between the two measurements is about 2.2σ, taking into account all uncorrelated uncertainties. Therefore, the measurements agree within their uncertainties. A small difference between the branching fractions of these two decays was already observed before by BESII, but the other way around [19].

The combined branching fraction is

$$\mathcal{B}(J/\psi \to p\bar{p}\eta) = (1.495 \pm 0.001 \pm 0.023) \times 10^{-3},$$

where the first uncertainty is the combined statistical uncertainty and the second one is the combined systematic uncertainty of both analyses. Correlations between both are taken into account. The combined result differs from the previous world average by 4.1σ. Former experiments used a pure three-body PHSP model for the determination of the global reconstruction efficiency. For this analysis, an amplitude analysis is performed to obtain better data/MC consistency. This causes part of the observed difference with the old experiments. The largest deviation from the pure three-body PHSP distribution was found to be caused by the destructive interference of the $N(1535)$ and the $N(1650)$ resonances.

In addition, the $p\bar{p}$ threshold region is studied. No evidence for any threshold enhancement in this channel is observed.

ACKNOWLEDGMENTS

The BESIII Collaboration thanks the staff of BEPCII and the IHEP computing center for their strong support. This work is supported in part by National Key R&D Program of China under Contracts No. 2020YFA0406300 and No. 2020YFA0406400; National Natural Science Foundation of China (NSFC) under Contracts No. 11635010, No. 11735014, No. 11835012, No. 11935015, No. 11935016, No. 11935018, No. 11961141012, No. 12025502, No. 12035009, No. 12035013, No. 12061131003, No. 12192260, No. 12192261, No. 12192262, No. 12192263, No. 12192264, No. 12192265, No. 12221005, No. 12225509, and No. 12235017; the Chinese Academy of Sciences (CAS) Large-Scale Scientific Facility Program; the CAS Center for Excellence in Particle Physics (CCEPP); Joint Large-Scale Scientific Facility Funds of the NSFC and CAS under Contract No. U1832207; CAS Key Research Program of Frontier Sciences under Contracts No. QYZDJ-SSW-SLH003 and No. QYZDJ-SSW-SLH040; 100 Talents Program of CAS; The Institute of Nuclear and Particle Physics (INPAC) and Shanghai Key Laboratory for Particle Physics and Cosmology; European Union's Horizon 2020 research and innovation programme under Marie Sklodowska-Curie grant agreement under Contract No. 894790; German Research Foundation DFG under Contract No. 455635585, Collaborative Research Center CRC 1044, Research Group No. FOR 5327, and Graduate School No. GRK 2149; Istituto Nazionale di Fisica Nucleare, Italy; Ministry of Development of Turkey under Contract No. DPT2006K-120470; National Research Foundation of Korea under Contract No. NRF-2022R1A2C1092335; National Science and Technology fund of Mongolia; National Science Research and Innovation Fund (NSRF) via the Program Management Unit for Human Resources & Institutional Development, Research and Innovation of Thailand under Contract No. B16F640076; Polish National Science Centre under Contract No. 2019/35/O/ST2/02907; The Swedish Research Council; and U.S. Department of Energy under Contract No. DE-FG02-05ER41374.

[1] M. Ronniger and B. C. Metsch, Eur. Phys. J. A **47**, 162 (2011).
[2] R. G. Edwards, J. J. Dudek, D. G. Richards, and S. J. Wallace, Phys. Rev. D **84**, 074508 (2011).
[3] R. L. Workman *et al.* (Particle Data Group), Prog. Theor. Exp. Phys. **2022**, 083C01 (2022).
[4] J. Z. Bai *et al.* (BES Collaboration), Phys. Rev. Lett. **91**, 022001 (2003).
[5] M. Ablikim *et al.* (BESIII Collaboration), Phys. Rev. Lett. **108**, 182001 (2012).
[6] J. Bai *et al.* (BES Collaboration), Phys. Lett. B **510**, 75 (2001).
[7] M. Ablikim *et al.* (BESIII Collaboration), Eur. Phys. J. C **53**, 15 (2008).
[8] M. Ablikim *et al.* (BESIII Collaboration), Phys. Rev. D **87**, 112004 (2013).
[9] J. P. Alexander *et al.* (CLEO Collaboration), Phys. Rev. D **82**, 092002 (2010).
[10] M. Ablikim *et al.* (BESIII Collaboration), Phys. Rev. Lett. **117**, 042002 (2016).
[11] M. Ablikim *et al.* (BESIII Collaboration), Phys. Rev. Lett. **106**, 072002 (2011).
[12] M. Ablikim *et al.* (BESIII Collaboration), Phys. Rev. Lett. **115**, 091803 (2015).
[13] X.-W. Kang, J. Haidenbauer, and U.-G. Meissner, Phys. Rev. D **91**, 074003 (2015).
[14] J.-P. Dedonder, B. Loiseau, and S. Wycech, Phys. Rev. C **97**, 065206 (2018).
[15] B. A. Li, Phys. Rev. D **74**, 034019 (2006).
[16] N. Kochelev and D.-P. Min, Phys. Lett. B **633**, 283 (2006).
[17] J. Bloms, AIP Conf. Proc. **2249**, 030029 (2020).
[18] V. Dmitriev, A. I. Milstein, and S. G. Salnikov, Phys. Lett. B **760**, 139 (2016).
[19] M. Ablikim *et al.* (BESIII Collaboration), Phys. Lett. B **676**, 25 (2009).
[20] M. Ablikim *et al.* (BESIII Collaboration), Nucl. Instrum. Methods Phys. Res., Sect. A **614**, 345 (2010).
[21] C. H. Yu *et al.*, *BEPCII Performance and Beam Dynamics Studies on Luminosity, IPAC2016* (JACoW, Geneva, Switzerland, 2016).
[22] X. L. Guo *et al.*, Radiat. Detect. Technol. Methods **3**, 14 (2019).
[23] X. Li *et al.*, Radiat. Detect. Technol. Methods **1**, 13 (2017).
[24] M. Ablikim *et al.* (BESIII Collaboration), Chin. Phys. C **46**, 074001 (2022).
[25] S. Jadach, B. F. L. Ward, and Z. Wąs, Comput. Phys. Commun. **130**, 260 (2000).
[26] D. J. Lange, Nucl. Instrum. Methods Phys. Res., Sect. A **462**, 152 (2001).
[27] R.-G. Ping, Chin. Phys. C **32**, 599 (2008).
[28] S. Agostinelli *et al.* (GEANT4 Collaboration), Nucl. Instrum. Methods Phys. Res., Sect. A **506**, 250 (2003).
[29] J. C. Chen, G. S. Huang, X. R. Qi, D. H. Zhang, and Y. S. Zhu, Phys. Rev. D **62**, 034003 (2000).
[30] R. L. Yang, R.-G. Ping, and H. Chen, Chin. Phys. Lett. **31**, 061301 (2014).
[31] M. Fritsch *et al.* (ComPWA Collaboration), 10.5281/zenodo.5526360; 10.5281/zenodo.5526648; and 10.5281/zenodo.5526650.
[32] R. Barlow, in *Conference on Advanced Statistical 37 Techniques in Particle Physics* (Advanced Statistical Techniques in Particle Physics, Durham, UK, 2002), p. 134.
[33] M. Ablikim *et al.* (BESIII Collaboration), Phys. Rev. D **89**, 074030 (2014).

M. Ablikim,[1] M. N. Achasov,[4,c] P. Adlarson,[75] O. Afedulidis,[3] X. C. Ai,[80] R. Aliberti,[35] A. Amoroso,[74a,74c] Q. An,[71,58,a] Y. Bai,[57] O. Bakina,[36] I. Balossino,[29a] Y. Ban,[46,h] H.-R. Bao,[63] V. Batozskaya,[1,44] K. Begzsuren,[32] N. Berger,[35] M. Berlowski,[44] M. Bertani,[28a] D. Bettoni,[29a] F. Bianchi,[74a,74c] E. Bianco,[74a,74c] A. Bortone,[74a,74c] I. Boyko,[36] R. A. Briere,[5] A. Brueggemann,[68] H. Cai,[76] X. Cai,[1,58] A. Calcaterra,[28a] G. F. Cao,[1,63] N. Cao,[1,63] S. A. Cetin,[62a] J. F. Chang,[1,58] G. R. Che,[43] G. Chelkov,[36,b] C. Chen,[43] C. H. Chen,[9] Chao Chen,[55] G. Chen,[1] H. S. Chen,[1,63] H. Y. Chen,[20] M. L. Chen,[1,58,63] S. J. Chen,[42] S. L. Chen,[45] S. M. Chen,[61] T. Chen,[1,63] X. R. Chen,[31,63] X. T. Chen,[1,63] Y. B. Chen,[1,58] Y. Q. Chen,[34] Z. J. Chen,[25,i] Z. Y. Chen,[1,63] S. K. Choi,[10] G. Cibinetto,[29a] F. Cossio,[74c] J. J. Cui,[50] H. L. Dai,[1,58] J. P. Dai,[78] A. Dbeyssi,[18] R. E. de Boer,[3] D. Dedovich,[36] C. Q. Deng,[72] Z. Y. Deng,[1] A. Denig,[35] I. Denysenko,[36] M. Destefanis,[74a,74c] F. De Mori,[74a,74c] B. Ding,[66,1] X. X. Ding,[46,h] Y. Ding,[34] Y. Ding,[40] J. Dong,[1,58] L. Y. Dong,[1,63] M. Y. Dong,[1,58,63] X. Dong,[76] M. C. Du,[1] S. X. Du,[80] Y. Y. Duan,[55] Z. H. Duan,[42] P. Egorov,[36,b] Y. H. Fan,[45] J. Fang,[59] J. Fang,[1,58] S. S. Fang,[1,63] W. X. Fang,[1] Y. Fang,[1] Y. Q. Fang,[1,58] R. Farinelli,[29a] L. Fava,[74b,74c] F. Feldbauer,[3] G. Felici,[28a] C. Q. Feng,[71,58] J. H. Feng,[59] Y. T. Feng,[71,58] M. Fritsch,[3] C. D. Fu,[1] J. L. Fu,[63] Y. W. Fu,[1,63] H. Gao,[63] X. B. Gao,[41] Y. N. Gao,[46,h] Yang Gao,[71,58] S. Garbolino,[74c] I. Garzia,[29a,29b] L. Ge,[80] P. T. Ge,[76] Z. W. Ge,[42] C. Geng,[59] E. M. Gersabeck,[67] A. Gilman,[69] K. Goetzen,[13] L. Gong,[40] W. X. Gong,[1,58] W. Gradl,[35] S. Gramigna,[29a,29b] M. Greco,[74a,74c] M. H. Gu,[1,58] Y. T. Gu,[15] C. Y. Guan,[1,63] A. Q. Guo,[31,63] L. B. Guo,[41] M. J. Guo,[50] R. P. Guo,[49] Y. P. Guo,[12,g] A. Guskov,[36,b] J. Gutierrez,[27] K. L. Han,[63] T. T. Han,[1] F. Hanisch,[3] X. Q. Hao,[19] F. A. Harris,[65] K. K. He,[55] K. L. He,[1,63] F. H. Heinsius,[3] C. H. Heinz,[35] Y. K. Heng,[1,58,63] C. Herold,[60] T. Holtmann,[3] P. C. Hong,[34] G. Y. Hou,[1,63] X. T. Hou,[1,63] Y. R. Hou,[63] Z. L. Hou,[1] B. Y. Hu,[59] H. M. Hu,[1,63] J. F. Hu,[56,j] S. L. Hu,[12,g] T. Hu,[1,58,63] Y. Hu,[1] G. S. Huang,[71,58] K. X. Huang,[59] L. Q. Huang,[31,63] X. T. Huang,[50] Y. P. Huang,[1]

Y. S. Huang,[59] T. Hussain,[73] F. Hölzken,[3] N. Hüsken,[35] N. in der Wiesche,[68] J. Jackson,[27] S. Jäger,[3] S. Janchiv,[32] J. H. Jeong,[10] Q. Ji,[1] Q. P. Ji,[19] W. Ji,[1,63] X. B. Ji,[1,63] X. L. Ji,[1,58] Y. Y. Ji,[50] X. Q. Jia,[50] Z. K. Jia,[71,58] D. Jiang,[1,63] H. B. Jiang,[76] P. C. Jiang,[46,h] S. S. Jiang,[39] T. J. Jiang,[16] X. S. Jiang,[1,58,63] Y. Jiang,[63] J. B. Jiao,[50] J. K. Jiao,[34] Z. Jiao,[23] S. Jin,[42] Y. Jin,[66] M. Q. Jing,[1,63] X. M. Jing,[63] T. Johansson,[75] S. Kabana,[33] N. Kalantar-Nayestanaki,[64] X. L. Kang,[9] X. S. Kang,[40] M. Kavatsyuk,[64] B. C. Ke,[80] V. Khachatryan,[27] A. Khoukaz,[68] R. Kiuchi,[1] O. B. Kolcu,[62a] B. Kopf,[3] M. Kuessner,[3] X. Kui,[1,63] N. Kumar,[26] A. Kupsc,[44,75] W. Kühn,[37] J. J. Lane,[67] P. Larin,[18] L. Lavezzi,[74a,74c] T. T. Lei,[71,58] Z. H. Lei,[71,58] M. Lellmann,[35] T. Lenz,[35] C. Li,[47] C. Li,[43] C. H. Li,[39] Cheng Li,[71,58] D. M. Li,[80] F. Li,[1,58] G. Li,[1] H. B. Li,[1,63] H. J. Li,[19] H. N. Li,[56,j] Hui Li,[43] J. R. Li,[61] J. S. Li,[59] K. Li,[1] L. J. Li,[1,63] L. K. Li,[1] Lei Li,[48] M. H. Li,[43] P. R. Li,[38,k,l] Q. M. Li,[1,63] Q. X. Li,[50] R. Li,[17,31] S. X. Li,[12] T. Li,[50] W. D. Li,[1,63] W. G. Li,[1,a] X. Li,[1,63] X. H. Li,[71,58] X. L. Li,[50] X. Y. Li,[1,63] X. Z. Li,[59] Y. G. Li,[46,h] Z. J. Li,[59] Z. Y. Li,[78] C. Liang,[42] H. Liang,[71,58] H. Liang,[1,63] Y. F. Liang,[54] Y. T. Liang,[31,63] G. R. Liao,[14] L. Z. Liao,[50] Y. P. Liao,[1,63] J. Libby,[26] A. Limphirat,[60] C. C. Lin,[55] D. X. Lin,[31,63] T. Lin,[1] B. J. Liu,[1] B. X. Liu,[76] C. Liu,[34] C. X. Liu,[1] F. Liu,[1] F. H. Liu,[53] Feng Liu,[6] G. M. Liu,[56,j] H. Liu,[38,k,l] H. B. Liu,[15] H. H. Liu,[1] H. M. Liu,[1,63] Huihui Liu,[21] J. B. Liu,[71,58] J. Y. Liu,[1,63] K. Liu,[38,k,l] K. Y. Liu,[40] Ke Liu,[22] L. Liu,[71,58] L. C. Liu,[43] Lu Liu,[43] M. H. Liu,[12,g] P. L. Liu,[1] Q. Liu,[63] S. B. Liu,[71,58] T. Liu,[12,g] W. K. Liu,[43] W. M. Liu,[71,58] X. Liu,[39] X. Liu,[38,k,l] Y. Liu,[38,k,l] Y. Liu,[80] Y. B. Liu,[43] Z. A. Liu,[1,58,63] Z. D. Liu,[9] Z. Q. Liu,[50] X. C. Lou,[1,58,63] F. X. Lu,[59] H. J. Lu,[23] J. G. Lu,[1,58] X. L. Lu,[1] Y. Lu,[7] Y. P. Lu,[1,58] Z. H. Lu,[1,63] C. L. Luo,[41] J. R. Luo,[59] M. X. Luo,[79] T. Luo,[12,g] X. L. Luo,[1,58] X. R. Lyu,[63] Y. F. Lyu,[43] F. C. Ma,[40] H. Ma,[78] H. L. Ma,[1] J. L. Ma,[1,63] L. L. Ma,[50] M. M. Ma,[1,63] Q. M. Ma,[1] R. Q. Ma,[1,63] T. Ma,[71,58] X. T. Ma,[1,63] X. Y. Ma,[1,58] Y. Ma,[46,h] Y. M. Ma,[31] F. E. Maas,[18] M. Maggiora,[74a,74c] S. Malde,[69] Y. J. Mao,[46,h] Z. P. Mao,[1] S. Marcello,[74a,74c] Z. X. Meng,[66] J. G. Messchendorp,[13,64] G. Mezzadri,[29a] H. Miao,[1,63] T. J. Min,[42] R. E. Mitchell,[27] X. H. Mo,[1,58,63] B. Moses,[27] N. Yu. Muchnoi,[4,c] J. Muskalla,[35] Y. Nefedov,[36] F. Nerling,[18,e] L. S. Nie,[20] I. B. Nikolaev,[4,c] Z. Ning,[1,58] S. Nisar,[11,m] Q. L. Niu,[38,k,l] W. D. Niu,[55] Y. Niu,[50] S. L. Olsen,[63] Q. Ouyang,[1,58,63] S. Pacetti,[28b,28c] X. Pan,[55] Y. Pan,[57] A. Pathak,[34] P. Patteri,[28a] Y. P. Pei,[71,58] M. Pelizaeus,[3] H. P. Peng,[71,58] Y. Y. Peng,[38,k,l] K. Peters,[13,e] J. L. Ping,[41] R. G. Ping,[1,63] S. Plura,[35] V. Prasad,[33] F. Z. Qi,[1] H. Qi,[71,58] H. R. Qi,[61] M. Qi,[42] T. Y. Qi,[12,g] S. Qian,[1,58] W. B. Qian,[63] C. F. Qiao,[63] X. K. Qiao,[80] J. J. Qin,[72] L. Q. Qin,[14] L. Y. Qin,[71,58] X. S. Qin,[50] Z. H. Qin,[1,58] J. F. Qiu,[1] Z. H. Qu,[72] C. F. Redmer,[35] K. J. Ren,[39] A. Rivetti,[74c] M. Rolo,[74c] G. Rong,[1,63] Ch. Rosner,[18] S. N. Ruan,[43] N. Salone,[44] A. Sarantsev,[36,d] Y. Schelhaas,[35] K. Schoenning,[75] M. Scodeggio,[29a] K. Y. Shan,[12,g] W. Shan,[24] X. Y. Shan,[71,58] Z. J. Shang,[38,k,l] J. F. Shangguan,[55] L. G. Shao,[1,63] M. Shao,[71,58] C. P. Shen,[12,g] H. F. Shen,[1,8] W. H. Shen,[63] X. Y. Shen,[1,63] B. A. Shi,[63] H. Shi,[71,58] H. C. Shi,[71,58] J. L. Shi,[12,g] J. Y. Shi,[1] Q. Q. Shi,[55] S. Y. Shi,[72] X. Shi,[1,58] J. J. Song,[19] T. Z. Song,[59] W. M. Song,[34,1] Y. J. Song,[12,g] Y. X. Song,[46,h,n] S. Sosio,[74a,74c] S. Spataro,[74a,74c] F. Stieler,[35] Y. J. Su,[63] G. B. Sun,[76] G. X. Sun,[1] H. Sun,[63] H. K. Sun,[1] J. F. Sun,[19] K. Sun,[61] L. Sun,[76] S. S. Sun,[1,63] T. Sun,[51,f] W. Y. Sun,[34] Y. Sun,[9] Y. J. Sun,[71,58] Y. Z. Sun,[1] Z. Q. Sun,[1,63] Z. T. Sun,[50] C. J. Tang,[54] G. Y. Tang,[1] J. Tang,[59] M. Tang,[71,58] Y. A. Tang,[76] L. Y. Tao,[72] Q. T. Tao,[25,i] M. Tat,[69] J. X. Teng,[71,58] V. Thoren,[75] W. H. Tian,[59] Y. Tian,[31,63] Z. F. Tian,[76] I. Uman,[62b] Y. Wan,[55] S. J. Wang,[50] B. Wang,[1] B. L. Wang,[63] Bo Wang,[71,58] D. Y. Wang,[46,h] F. Wang,[72] H. J. Wang,[38,k,l] J. J. Wang,[76] J. P. Wang,[50] K. Wang,[1,58] L. L. Wang,[1] M. Wang,[50] N. Y. Wang,[63] S. Wang,[38,k,l] S. Wang,[12,g] T. Wang,[12,g] T. J. Wang,[43] W. Wang,[72] W. Wang,[59] W. P. Wang,[35,71,o] X. Wang,[46,h] X. F. Wang,[38,k,l] X. J. Wang,[39] X. L. Wang,[12,g] X. N. Wang,[1] Y. Wang,[61] Y. D. Wang,[45] Y. F. Wang,[1,58,63] Y. L. Wang,[19] Y. N. Wang,[45] Y. Q. Wang,[1] Yaqian Wang,[17] Yi Wang,[61] Z. Wang,[1,58] Z. L. Wang,[72] Z. Y. Wang,[1,63] Ziyi Wang,[63] D. H. Wei,[14] F. Weidner,[68] S. P. Wen,[1] Y. R. Wen,[39] U. Wiedner,[3] G. Wilkinson,[69] M. Wolke,[75] L. Wollenberg,[3] C. Wu,[39] J. F. Wu,[1,8] L. H. Wu,[1] L. J. Wu,[1,63] X. Wu,[12,g] X. H. Wu,[34] Y. Wu,[71,58] Y. H. Wu,[55] Y. J. Wu,[31] Z. Wu,[1,58] L. Xia,[71,58] X. M. Xian,[39] B. H. Xiang,[1,63] T. Xiang,[46,h] D. Xiao,[38,k,l] G. Y. Xiao,[42] S. Y. Xiao,[1] Y. L. Xiao,[12,g] Z. J. Xiao,[41] C. Xie,[42] X. H. Xie,[46,h] Y. Xie,[50] Y. G. Xie,[1,58] Y. H. Xie,[6] Z. P. Xie,[71,58] T. Y. Xing,[1,63] C. F. Xu,[1,63] C. J. Xu,[59] G. F. Xu,[1] H. Y. Xu,[66,2,p] M. Xu,[71,58] Q. J. Xu,[16] Q. N. Xu,[30] W. Xu,[1] W. L. Xu,[66] X. P. Xu,[55] Y. C. Xu,[77] Z. P. Xu,[42] Z. S. Xu,[63] F. Yan,[12,g] L. Yan,[12,g] W. B. Yan,[71,58] W. C. Yan,[80] X. Q. Yan,[1] H. J. Yang,[51,f] H. L. Yang,[34] H. X. Yang,[1] T. Yang,[1] Y. Yang,[12,g] Y. F. Yang,[1,63] Y. F. Yang,[43] Y. X. Yang,[1,63] Z. W. Yang,[38,k,l] Z. P. Yao,[50] M. Ye,[1,58] M. H. Ye,[8] J. H. Yin,[1] Z. Y. You,[59] B. X. Yu,[1,58,63] C. X. Yu,[43] G. Yu,[1,63] J. S. Yu,[25,i] T. Yu,[72] X. D. Yu,[46,h] Y. C. Yu,[80] C. Z. Yuan,[1,63] J. Yuan,[34] J. Yuan,[45] L. Yuan,[2] S. C. Yuan,[1,63] Y. Yuan,[1,63] Z. Y. Yuan,[59] C. X. Yue,[39] A. A. Zafar,[73] F. R. Zeng,[50] S. H. Zeng,[72] X. Zeng,[12,g] Y. Zeng,[25,i] Y. J. Zeng,[59] Y. J. Zeng,[1,63] X. Y. Zhai,[34] Y. C. Zhai,[50] Y. H. Zhan,[59] A. Q. Zhang,[1,63] B. L. Zhang,[1,63] B. X. Zhang,[1] D. H. Zhang,[43] G. Y. Zhang,[19] H. Zhang,[80] H. Zhang,[71,58] H. C. Zhang,[1,58,63] H. H. Zhang,[34] H. H. Zhang,[59] H. Q. Zhang,[1,58,63] H. R. Zhang,[71,58] H. Y. Zhang,[1,58] J. Zhang,[80] J. Zhang,[59] J. J. Zhang,[52]

J. L. Zhang,[20] J. Q. Zhang,[41] J. S. Zhang,[12,g] J. W. Zhang,[1,58,63] J. X. Zhang,[38,k,l] J. Y. Zhang,[1] J. Z. Zhang,[1,63] Jianyu Zhang,[63] L. M. Zhang,[61] Lei Zhang,[42] P. Zhang,[1,63] Q. Y. Zhang,[34] R. Y. Zhang,[38,k,l] S. H. Zhang,[1,63] Shulei Zhang,[25,i] X. D. Zhang,[45] X. M. Zhang,[1] X. Y. Zhang,[50] Y. Zhang,[72] Y. Zhang,[1] Y. T. Zhang,[80] Y. H. Zhang,[1,58] Y. M. Zhang,[39] Yan Zhang,[71,58] Z. D. Zhang,[1] Z. H. Zhang,[1] Z. L. Zhang,[34] Z. Y. Zhang,[76] Z. Y. Zhang,[43] Z. Z. Zhang,[45] G. Zhao,[1] J. Y. Zhao,[1,63] J. Z. Zhao,[1,58] L. Zhao,[1] Lei Zhao,[71,58] M. G. Zhao,[43] N. Zhao,[78] R. P. Zhao,[63] S. J. Zhao,[80] Y. B. Zhao,[1,58] Y. X. Zhao,[31,63] Z. G. Zhao,[71,58] A. Zhemchugov,[36,b] B. Zheng,[72] B. M. Zheng,[34] J. P. Zheng,[1,58] W. J. Zheng,[1,63] Y. H. Zheng,[63] B. Zhong,[41] X. Zhong,[59] H. Zhou,[50] J. Y. Zhou,[34] L. P. Zhou,[1,63] S. Zhou,[6] X. Zhou,[76] X. K. Zhou,[6] X. R. Zhou,[71,58] X. Y. Zhou,[39] Y. Z. Zhou,[12,g] J. Zhu,[43] K. Zhu,[1] K. J. Zhu,[1,58,63] K. S. Zhu,[12,g] L. Zhu,[34] L. X. Zhu,[63] S. H. Zhu,[70] S. Q. Zhu,[42] T. J. Zhu,[12,g] W. D. Zhu,[41] Y. C. Zhu,[71,58] Z. A. Zhu,[1,63] J. H. Zou,[1] and J. Zu[71,58]

(BESIII Collaboration)

[1]*Institute of High Energy Physics, Beijing 100049, People's Republic of China*
[2]*Beihang University, Beijing 100191, People's Republic of China*
[3]*Bochum Ruhr-University, D-44780 Bochum, Germany*
[4]*Budker Institute of Nuclear Physics SB RAS (BINP), Novosibirsk 630090, Russia*
[5]*Carnegie Mellon University, Pittsburgh, Pennsylvania 15213, USA*
[6]*Central China Normal University, Wuhan 430079, People's Republic of China*
[7]*Central South University, Changsha 410083, People's Republic of China*
[8]*China Center of Advanced Science and Technology, Beijing 100190, People's Republic of China*
[9]*China University of Geosciences, Wuhan 430074, People's Republic of China*
[10]*Chung-Ang University, Seoul 06974, Republic of Korea*
[11]*COMSATS University Islamabad, Lahore Campus, Defence Road, Off Raiwind Road, 54000 Lahore, Pakistan*
[12]*Fudan University, Shanghai 200433, People's Republic of China*
[13]*GSI Helmholtzcentre for Heavy Ion Research GmbH, D-64291 Darmstadt, Germany*
[14]*Guangxi Normal University, Guilin 541004, People's Republic of China*
[15]*Guangxi University, Nanning 530004, People's Republic of China*
[16]*Hangzhou Normal University, Hangzhou 310036, People's Republic of China*
[17]*Hebei University, Baoding 071002, People's Republic of China*
[18]*Helmholtz Institute Mainz, Staudinger Weg 18, D-55099 Mainz, Germany*
[19]*Henan Normal University, Xinxiang 453007, People's Republic of China*
[20]*Henan University, Kaifeng 475004, People's Republic of China*
[21]*Henan University of Science and Technology, Luoyang 471003, People's Republic of China*
[22]*Henan University of Technology, Zhengzhou 450001, People's Republic of China*
[23]*Huangshan College, Huangshan 245000, People's Republic of China*
[24]*Hunan Normal University, Changsha 410081, People's Republic of China*
[25]*Hunan University, Changsha 410082, People's Republic of China*
[26]*Indian Institute of Technology Madras, Chennai 600036, India*
[27]*Indiana University, Bloomington, Indiana 47405, USA*
[28a]*INFN Laboratori Nazionali di Frascati, INFN Laboratori Nazionali di Frascati, I-00044 Frascati, Italy*
[28b]*INFN Sezione di Perugia, I-06100 Perugia, Italy*
[28c]*University of Perugia, I-06100 Perugia, Italy*
[29a]*INFN Sezione di Ferrara, INFN Sezione di Ferrara, I-44122 Ferrara, Italy*
[29b]*University of Ferrara, I-44122 Ferrara, Italy*
[30]*Inner Mongolia University, Hohhot 010021, People's Republic of China*
[31]*Institute of Modern Physics, Lanzhou 730000, People's Republic of China*
[32]*Institute of Physics and Technology, Peace Avenue 54B, Ulaanbaatar 13330, Mongolia*
[33]*Instituto de Alta Investigación, Universidad de Tarapacá, Casilla 7D, Arica 1000000, Chile*
[34]*Jilin University, Changchun 130012, People's Republic of China*
[35]*Johannes Gutenberg University of Mainz, Johann-Joachim-Becher-Weg 45, D-55099 Mainz, Germany*
[36]*Joint Institute for Nuclear Research, 141980 Dubna, Moscow region, Russia*
[37]*Justus-Liebig-Universitaet Giessen, II. Physikalisches Institut, Heinrich-Buff-Ring 16, D-35392 Giessen, Germany*
[38]*Lanzhou University, Lanzhou 730000, People's Republic of China*
[39]*Liaoning Normal University, Dalian 116029, People's Republic of China*

[40]Liaoning University, Shenyang 110036, People's Republic of China
[41]Nanjing Normal University, Nanjing 210023, People's Republic of China
[42]Nanjing University, Nanjing 210093, People's Republic of China
[43]Nankai University, Tianjin 300071, People's Republic of China
[44]National Centre for Nuclear Research, Warsaw 02-093, Poland
[45]North China Electric Power University, Beijing 102206, People's Republic of China
[46]Peking University, Beijing 100871, People's Republic of China
[47]Qufu Normal University, Qufu 273165, People's Republic of China
[48]Renmin University of China, Beijing 100872, People's Republic of China
[49]Shandong Normal University, Jinan 250014, People's Republic of China
[50]Shandong University, Jinan 250100, People's Republic of China
[51]Shanghai Jiao Tong University, Shanghai 200240, People's Republic of China
[52]Shanxi Normal University, Linfen 041004, People's Republic of China
[53]Shanxi University, Taiyuan 030006, People's Republic of China
[54]Sichuan University, Chengdu 610064, People's Republic of China
[55]Soochow University, Suzhou 215006, People's Republic of China
[56]South China Normal University, Guangzhou 510006, People's Republic of China
[57]Southeast University, Nanjing 211100, People's Republic of China
[58]State Key Laboratory of Particle Detection and Electronics, Beijing 100049, Hefei 230026, People's Republic of China
[59]Sun Yat-Sen University, Guangzhou 510275, People's Republic of China
[60]Suranaree University of Technology, University Avenue 111, Nakhon Ratchasima 30000, Thailand
[61]Tsinghua University, Beijing 100084, People's Republic of China
[62a]Turkish Accelerator Center Particle Factory Group, Istinye University, 34010 Istanbul, Turkey
[62b]Near East University, Nicosia, North Cyprus, 99138, Mersin 10, Turkey
[63]University of Chinese Academy of Sciences, Beijing 100049, People's Republic of China
[64]University of Groningen, NL-9747 AA Groningen, Netherlands
[65]University of Hawaii, Honolulu, Hawaii 96822, USA
[66]University of Jinan, Jinan 250022, People's Republic of China
[67]University of Manchester, Oxford Road, Manchester M13 9PL, United Kingdom
[68]University of Muenster, Wilhelm-Klemm-Strasse 9, 48149 Muenster, Germany
[69]University of Oxford, Keble Road, Oxford OX13RH, England, United Kingdom
[70]University of Science and Technology Liaoning, Anshan 114051, People's Republic of China
[71]University of Science and Technology of China, Hefei 230026, People's Republic of China
[72]University of South China, Hengyang 421001, People's Republic of China
[73]University of the Punjab, Lahore-54590, Pakistan
[74a]University of Turin and INFN, University of Turin, I-10125 Turin, Italy
[74b]University of Eastern Piedmont, I-15121 Alessandria, Italy
[74c]INFN, I-10125 Turin, Italy
[75]Uppsala University, Box 516, SE-75120 Uppsala, Sweden
[76]Wuhan University, Wuhan 430072, People's Republic of China
[77]Yantai University, Yantai 264005, People's Republic of China
[78]Yunnan University, Kunming 650500, People's Republic of China
[79]Zhejiang University, Hangzhou 310027, People's Republic of China
[80]Zhengzhou University, Zhengzhou 450001, People's Republic of China

[a]Deceased.
[b]Also at the Moscow Institute of Physics and Technology, Moscow 141700, Russia.
[c]Also at the Novosibirsk State University, Novosibirsk 630090, Russia.
[d]Also at the NRC "Kurchatov Institute", PNPI, 188300 Gatchina, Russia.
[e]Also at Goethe University Frankfurt, 60323 Frankfurt am Main, Germany.
[f]Also at Key Laboratory for Particle Physics, Astrophysics and Cosmology, Ministry of Education; Shanghai Key Laboratory for Particle Physics and Cosmology; Institute of Nuclear and Particle Physics, Shanghai 200240, China.
[g]Also at Key Laboratory of Nuclear Physics and Ion-beam Application (MOE) and Institute of Modern Physics, Fudan University, Shanghai 200443, China.
[h]Also at State Key Laboratory of Nuclear Physics and Technology, Peking University, Beijing 100871, China.
[i]Also at School of Physics and Electronics, Hunan University, Changsha 410082, China.
[j]Also at Guangdong Provincial Key Laboratory of Nuclear Science, Institute of Quantum Matter, South China Normal University, Guangzhou 510006, China.

[k]Also at MOE Frontiers Science Center for Rare Isotopes, Lanzhou University, Lanzhou 730000, China.
[l]Also at Lanzhou Center for Theoretical Physics, Lanzhou University, Lanzhou 730000, China.
[m]Also at the Department of Mathematical Sciences, IBA, Karachi 75270, Pakistan.
[n]Also at Ecole Polytechnique Federale de Lausanne (EPFL), CH-1015 Lausanne, Switzerland.
[o]Also at Helmholtz Institute Mainz, Staudinger Weg 18, D-55099 Mainz, Germany.
[p]Also at School of Physics, Beihang University, Beijing 100191, China.